PREFRONTAL CONNECTIONS OF THE PERIRHINAL AND POSTRHINAL CORTICES IN THE RAT

Eunkyu Hwang¹, Bailey S. Willis², and Rebecca D. Burwell^{1,3}

¹Departments of Cognitive, Linguistic, and Psychological Sciences, of ²Molecular Pharmacology, Physiology, and Biotechnology and of ³Neuroscience

Brown University, Providence, RI, 02912 USA

Number of Words: 11,684

Number of Figures: 6

Number of Tables: 5

Abbreviated Title: Prefrontal Connections of the rodent parahippocampal region

Please direct correspondence and reprint requests to:
Rebecca D. Burwell, Ph.D.
Department of Cognitive, Linguistic, and Psychological Sciences
Brown University
190 Thayer St.
Providence, RI 02912 USA

phone: 011-1-401-863-9208 fax: 011-1-401-863-1300

email: Rebecca Burwell@Brown.edu

Abstract

Knowing how prefrontal regions interact with medial temporal lobe structures is important for understanding memory and cognition. Using anterograde and retrograde tract

tracing methods in the rat, we report a detailed study of the perirhinal (PER) and postrhinal (POR) connections with the lateral, ventrolateral, and medial orbitofrontal cortices (ORBI, ORBvI, ORBm), infralimbic and prelimbic cortices (IL, PL), ventral and dorsal anterior cingulate cortices (ACAv, ACAd), and secondary motor cortex (MOs). Our analyses included the topography and laminar patterns of these connections. The PER and POR showed reciprocal connectivity with all prefrontal regions examined, but the patterns of connections differed. In general, PER areas 36 and 35 showed patterns of connectivity that were more similar to each other than to those of the POR. Analysis of anterograde tracers showed that PER areas 36 and 35 provide the strongest projections to prefrontal regions. The heaviest fiber labeling was in IL and PL, closely followed by orbital regions. Fiber labeling arising from injections in POR was weaker overall. The strongest POR efferents targeted MOs, ACAv, and ORBvl. For return projections, analysis of retrograde tracers showed that PER areas 36 and 35 receive strong inputs from orbitofrontal and medial prefrontal regions. Interestingly, PER also received substantial inputs from MOs and ACAd. The POR receives a very strong input from MOs, followed by ACAd, and ORBvl. Based on comparison of our findings with those obtained in monkeys, we argue that the rodent ACAd and MOs may be a functional homolog of the primate dorsolateral prefrontal cortex.

Highlights (3-5, 85 char w spaces)

- We examined the frontal and prefrontal connections of perirhinal and postrhinal cortex.
- Perirhinal is preferentially connected with medial prefrontal areas.
- Postrhinal cortex is preferentially connected with secondary motor cortex, which may be the rodent homolog of the primate dorsolateral prefrontal cortex

Keywords

Neuroanatomical; tract tracing; parahippocampal cortex; dorsolateral prefrontal cortex

1. Introduction

The primate medial temporal lobe (MTL) comprises the hippocampal formation (dentate gyrus, hippocampal fields CA3, CA2, CA1, and subiculum) and the parahippocampal region (entorhinal cortex, perirhinal cortex (PER), parahippocampal cortex (PHC), and the pre- and parasubiculum) [1]. The PER and the POR in rodents are the functional homologs of the PER and the PHC in primates, respectively [2]. The parahippocampal regions of both primates and rodents provide unimodal and polymodal associational input to the hippocampus. Anatomical inputs to the PER suggest that the region might be important for visual object recognition memory, whereas the inputs to the POR/PHC suggest a role in spatial functions [3, 4]. These findings prompted a view of MTL positing that the PER provides object and item information to the hippocampus (HC) and the POR provides spatial and contextual information [5]. It is clear, however, that the PER and the POR do more than merely convey sensory information to the hippocampus. Rather, they have important functions of their own. Given the substantial differences in anatomical connections, it should not be surprising that the PER and POR support different functions, or that the two regions interact to support some cognitive tasks [6]. Available evidence suggests that prefrontal cortical regions (PFC) are also involved in contextguided and novelty-guided behavior [reviewed in 7, 8-11]. Thus understanding the PFC connections of the PER and POR will facilitate studies of the functional circuitry underlying the use of context and novelty to guide appropriate behavior.

Anatomical studies suggest that the PER and the POR/PHC show good homology across mice, rats, monkeys, and humans [12-15]. There is also a good case for rodent-primate homology across frontal areas for most regions [16-18, but see 19]. The prefrontal cortex in the rat brain comprises several brain areas including orbitofrontal regions (ORB), medial prefrontal regions including the infralimbic and prelimbic cortices (IL, PL), ventral and dorsal anterior cingulate cortices (ACAv, ACAd), and secondary motor cortex (MOs, Figure 1). There is good

evidence for homology across orbital and medial PFC [16, 17]. The case for ACA is less clear, although one suggestion is that the rodent medial PFC exhibits some functions of the primate ACA [18]. Another suggestion is that ACAd exhibits some functions of the ventral part of the primate dorsolateral PFC (DLPFC) [20].

The primate DLPFC is a region of particular interest with respect to rodent-primate homology. In monkeys, this region receives strong input from the PHC [4]. DLPFC in monkeys and humans is widely thought to be involved in monitoring and other executive control functions [reviewed in 21]. Interestingly, MOs in the rodent plays an important role in processing sensory information in order to guide appropriate goal-directed behavior [22]. This region has been studied under a variety of names, including secondary motor cortex (M2, AGm, and Fr2), shoulder cortex, and rat frontal eye fields [reviewed in 7]. Damaging MOs seems to disrupt motor responses driven by sensory input [23] and impairs motor learning, but not execution of motor responses [24]. Taken together, these findings suggest MOs could be the rodent homolog of primate dorsolateral PFC. Based on a comparison of the anatomy of prefrontal cortex in rats and primates, Uylings and van Eden [25] concluded that a portion of MOs is the functional homolog of the primate DLPFC, and Kesner [26] suggested that anterior cingulate cortex is homologous to DLPFC [but see 18, 19]. Uylings and colleagues [27] assessed the case for prefrontal homology across rats and nonhuman primates and asserted that there is homology for medial, orbital, and dorsolateral prefrontal areas. They concluded that that MOs and ACAd have more prefrontal than premotor connectional characteristics. This so-called "shoulder" region receives more input from retrosplenial cortex and visual areas than from motor areas. Uylings and colleagues further suggested, based on electrophysiology and experimental lesion studies, that caudal MOs and parts of ACAd comprise a zone homologous to the macaque frontal eye field. If MOs is the rodent homolog of DLPFC, we would expect to see strong connectivity with PER and POR.

In a series of quantitative and semiquantitative neuroanatomical studies, we previously reported connections of the PER, POR, and lateral and medial entorhinal cortices of the rat for about seventy efferent and afferent regions [3, 28-31]. These studies provide the framework for the present study in which we provide more detailed analyses of the topographical and laminar patterns of connections of the POR and PER areas 35 and 36 with the PFC.

2. Nomenclature

We analyzed the connections of the PER and POR with a total of eight prefrontal regions (Figures 1B and 2). These regions included medial prefrontal regions, prelimbic area (PL) and infralimbic area (ILA), the medial, ventrolateral, and lateral orbital areas (ORBm, ORBvl, and ORBl, respectively), dorsal and ventral anterior cingulate cortices (ACAd and ACAv), and supplementary motor cortex (MOs). Unless otherwise specified, we relied largely on Swanson [32] and Krettek and Price [33] to identify the borders of the prefrontal regions using cytoarchitectonic features. Borders and cytoarchitectonic features of MOs were from Donoghue and Wise [34]. MOs was included in our analyses because it receives input from the mediodorsal nucleus of the thalamus [33, 35]; such input is characteristic of prefrontal cortex [36]. Another reason for including MOs is the possibility that some aspect of the region may be a functional homolog of the primate dorsolateral PFC [25].

Borders and histological criteria for the PER and POR are according to Burwell [13]. Briefly, the PER is located in and near the rhinal fissure, and comprises two subregions, the dorsally situated area 36 and the ventrally situated area 35 (Figure 1A). The POR forms the caudal border of the PER and lies dorsal to the caudal extension of the rhinal sulcus. Rostral PER occupies the rhinal sulcus, but as the region extends caudally, more and more of PER is located above the sulcus. The POR is almost entirely dorsal to the sulcus. All three regions have been further subdivided, but for the purposes of these analyses, we assessed connections for PER areas 35 and 36 and for the POR.

In Brodmann's [37] nomenclature, area 35 was also termed perirhinal cortex and area 36 was also termed ectorhinal cortex. Currently, the most commonly used nomenclature for memory research in the primate brain is the PER comprising areas 35 and 36. Burwell and colleagues [2, 13] adapted that nomenclature for use in the rodent brain. The term ectorhinal is no longer in use except in rodent brain atlases. Thus, within a comparative framework for experimental neuroscience, it seems reasonable to adhere to the nomenclature of perirhinal cortex as designating the combined areas 35 and 36 for both the rodent and primate brains.

Despite the many anatomical and functional studies of the POR in rats and mice, currently available atlases of the rodent brain do not recognize the POR as a separate region. In the available rodent atlas's a close approximation of the POR would comprise the caudal extents of the perirhinal cortex, ectorhinal cortex, and the ventral third of the dorsally adjacent ventral temporal cortex that are located caudal to the emergence of the angular bundle. This is the level at which the dentate gyrus is no longer apparent in the coronal plane [32, 38]. Best practice, however, would be to augment the use of an atlas with studies of POR cytoarchitecture and borders [12, 13].

3. Materials and methods

3.1. Subjects

Subjects were 29 Sprague-Dawley rats for the anterograde study and 46 male Sprague-Dawley rats for the retrograde study (Harlan Laboratories, Houston, TX). Subjects were 2-3 months of age and weighed between 300 and 400g at the time of surgery. Prior to surgery, animals were housed in pairs or individually under a standard 12 h light/ 12 h dark cycle with *ad libitum* access to water and food. Post-surgery, all animals were housed individually. All methods involving the use of live subjects were approved by the appropriate institutional animal care and use committee and followed NIH guidelines.

From a library of 42 cases, we chose for analysis ten anterograde cases and 19 retrograde cases. Data from these cases were previously analyzed for other anatomical studies [3, 28-30, 39, 40]. The earlier studies quantified overall strength of labeling for larger numbers of efferent and afferent regions, but included little information about the topographical and laminar patterns of labeling observed in these regions including the prefrontal cortex. The present study builds on the earlier work by providing detailed analyses of the topography and laminar patterns of connections of the PER and POR with PFC regions.

3.2. Surgery

Surgery was performed as previously reported [3, 29, 39]. Animals were anesthetized with sodium pentobarbital (Nembutal, Abbott Laboratories, North Chicago, IL, 50mg/kg, i.p) or with inhalation anesthetic (halothane or isoflurane) and placed in a stereotaxic apparatus (Kopf, Tujunga, CA). An incision was made in the scalp and the connective tissue was retracted. Using a dental drill, craniotomies were made in the skull dorsal to the intended injection sites. A small incision was then made in the dura to allow insertion of the micropipette without breakage. Each subject received from one to three injections of anterograde and/or retrograde tract tracers.

Tracers were injected at various locations in the PER and the POR.

For the anterograde studies, we used Biotinylated dextran amine (BDA, Molecular Probes, Eugene OR) and *Phaseolus vulgaris*-leuccoagglutinin (PHA-L, Vector Laboratories, Burlingame CA). Tracers were delivered by ionophoresis, with 4 µA positive DC current, alternating between 8 s on and 8 s off for 8 min. We used glass micropipettes with tip diameters of 4-5µm. BDA was a 10% solution in 0.1 M phosphate buffered saline (PBS), and PHA-L was a 2.5% solution in 0.1 M PBS.

For the retrograde injections, we used Fast Blue (FB), Diamidino Yellow (DY), and Fluoro-gold (FG). Both FB and DY were acquired from Dr. Illing GmbH and Co. (Gross Umstadt, Germany). FG was acquired from FG, Flurochrome, Inc. (Englewood, CO). Tracers were pressure injected through a glass micropipettes with tip diameters ranging from 60 to 90 mm.

Tracer injection volumes and solutions were 200nl of 2% FB in distilled H_2O , 150 nl of 3% DY in distilled H_2O , or 100 nl of a 2% FG in normal saline. The rate of injection was 30 nl/minute. Immediately following the injection, the micropipette was raised 100 μ m. After a 10-minute wait, the micropipette was slowly raised at a rate of approximately 500 μ m/minute.

Following tracer injection, the wound was sutured, and the animal was visually monitored, periodically, for several hours. Once subjects were awake and had demonstrated the righting reflex, they were returned to the colony for a variable survival period depending on the tracers injected. Survival was 7–14 days.

3.3 Tissue processing

3.3.1 Perfusion and sectioning

After the survival period, animals were anesthetized with an intraperitoneal injection of Beuthanasia (Schering-Plough, Kenilworth, NJ) or a 35% solution of chloral hydrate. Animals were transcardially perfused using a pH-shift protocol at a flow rate of 35-40 ml/min. Room temperature saline was perfused for two minutes, followed by 10 minutes of 4% paraformaldehyde in 0.1M sodium acetate buffer (pH 6.5 at 4° C) and 15 minutes of 4% paraformaldehyde in 0.1M sodium borate buffer (pH 9.5 at 4° C). During perfusion, ice was packed around the animal's head. Brains were removed from the skull, postfixed for 6 hours in the paraformaldehyde-sodium borate solution, and cryoprotected for 24 hours in 20% glycerol in 0.02 M potassium PBS (KPBS, pH 7.4 at 4° C). Brains were then blocked and frozen for immediate sectioning or stored at -80° C for later processing.

Brains were sectioned into five series of 30 µm sections on a freezing microtome. Sectioning began at the rostral limit of the prefrontal cortex and extended through the caudal pole of the neocortex. One or two series of the 1:5 series were used for retrograde and/or anterograde tracer processing. One series was mounted and stained for Nissl using thionin. The remaining series were either used for other procedures or were stored at -70°C in

cryoprotectant consisting of 30% ethylene glycol and 25% glycerol in sodium phosphate buffer [for details, see 39].

3.3.2 Anterograde tracers

To visualize BDA labeled fibers, we used an avidin-biotin reaction. Sections were pretreated in a 1% solution of Triton X-100 in KPBS for 1 hour to facilitate penetration of reagents. Sections were then incubated for 24 hours at 4°C in a solution of stabilizer (1:50 dilution) and avidin reagent (1:25 dilution) in KPBS plus 0.1% solution of Triton X-100. Sections were washed 3 x 10 minutes in KPBS. Next, sections were incubated in 0.05% 3,3'-DAB (Pierce, Tacoma, WA) and 0.04% hydrogen peroxide in KPBS for 10-30 minutes.

For visualization of PHA-L, we used two methods was used depending on whether there were one or two anterograde tract tracer injections [for details, see 39]. If only one tracer was present, we used a biotinylated secondary antibody, with an avidin-biotin incubation (adapted from Gerfen and Sawchenko 1984). Sections were first incubated for 2-3 hours in 5% normal goat serum (NGS) and 0.5% Triton X-100 in KPBS in order to minimize nonspecific binding. Sections were then incubated for 24-48 hours in the primary antiserum solution of rabbit anti-PHA-L (1:12000 dilution) in 0.3% Triton X-100 and 2% NGS in KPBS. Sections were washed twice for 10 minutes in 2% NGS in KPBS, and then incubated for 45 minutes in the biotinylated secondary antibody solution containing goat antirabbit IgG (1:277 dilution) in 0.3% Triton X-100, and 2% NGS in KPBS. Sections were then washed in 2% NGS in KPBS and incubated in 0.05% DAB and 0.04% hydrogen peroxide in KPBS for 5-10 minutes. If two tracers were present, a PAP complex was used rather than the avidin reagent. The procedure was identical, except that the secondary antiserum was goat antirabbit IgG at 1:2000 dilution followed by a rabbit PAP incubation.

Once all immunohistochemical processing was complete, sections were washed in KPBS and mounted on gelatin covered slides. Mounted sections were dried, defatted, and intensified with osmium tetroxide and thiocarbohydrate [41] or gold chloride [42]. For osmium

tetroxide intensification, slides were first hydrated through graded alcohols to distilled water. They were then incubated for 10-20 minutes in 0.005% OsO4 in distilled and deionized water (ddH₂O). Slides were washed for 30 minutes in running tap water followed by three dips in ddH₂O. Next slides were incubated for 5-15 minutes in 0.05% thiocarbohydrate in ddH₂O. Again, slides were washed for 30 minutes in running tap water followed by three dips in ddH₂O. Slides were transferred back to the original osmium solution for an additional 10-30 minutes followed by a 30 minutes tap water wash and ddH₂O rinse. For gold chloride intensification, slides were hydrated through graded alcohols and rinsed in ddH2O. Sections were incubated in the dark in acid washed glassware for 45 minutes at 56°C in a solution of 1% silver nitrate in distilled water (dH₂O). The silver nitrate solution was neutralized with 30% ammonium hydroxide in dH₂O by adding small drops until the pH reached 7.0 (check the pH with a pH strip). Slides were rinsed in running tap water for 2 minutes and dipped in dH₂O. Slides were then incubated in the dark for 10 minutes in a solution of 0.2% gold chloride in dH₂O at room temperature. Slides were again rinsed in running tap water for 2 minutes and dipped in dH₂O. To stabilize the silver-gold complex, slides were incubated in a 5% solution of sodium thiosulfate in dH20 for 10 minutes 56°C. Finally, slides were rinsed in running tap water for 2 minutes and dipped in dH20. Following intensification, slides were dehydrated in graded ethanols followed by xylene and coverslipped with DPX mountant (Gallard-Schlessinger, Plainview, NY).

3.3.3 Retrograde tracers

Sections analyzed for retrogradely transported fluorescence were mounted onto gelatin-coated slides on the same day of sectioning. The mounted tissue was dried for 2-4 hours at room temperature in an opaque vacuum dessicator, dehydrated in 100% ethanol (2x2 minutes), cleared in xylene (3x2 minutes), and cover slipped with DPX mountant.

3.4 Anatomical analysis

3.4.1 Anterograde tracers

Anterograde material was analyzed using a voxel approach. Using a Nikon E600 compound microscope coupled to a semi-automated data collection system (Neurolucida, Microbrightfield, Inc., Burlington, VT), digital contours were drawn from Nissl sections adjacent to the anterograde tracer sections. The contours included regional boundaries, cortical surface, and cortical layers of each frontal region analyzed. Contours were drawn for a 1:10 series of 30 µm coronal sections (300 µm intervals). The outline of the cortical surface was then subdivided into 600 µm segments. Lines were drawn perpendicular from the pial surface to the deep border of layer VI to create a series of cortical columns, divided into layers. These contours were then digitally overlaid onto a Neurolucida darkfield image of the corresponding BDA or PHA-L section for quantification of density of labeled fibers. The density of labeled fibers for different layers (I-III, V, and VI) within each column was determined according to a rating scale of 0 to 6. A score of 0 indicated no fibers were present, whereas a score of 6 denoted heavy density of labeled fibers.

Density of labeling was normalized across animals as previously described [28]. Briefly, criteria for scoring density of labeling from 0-6 were developed on a case by case basis, such that the heaviest density of labeled fibers observed for that case was set to a score of 6. For POR injection sites, the heaviest labeling found in entorhinal cortex or the PER was used to develop the criteria. For PER injection sites, entorhinal and POR labeling were used to develop the criteria. Thus, for a PER case, the heaviest labeling observed in the POR or entorhinal cortex would be set to 6. Density of fiber labeling was scored separately for layers I-III, V, and VI.

For each case and for each prefrontal region analyzed, the density ratings for the cortical columns and for each layer were entered into cells of a Microsoft Excel spreadsheet, beginning with the most anterior coronal section in which the region appeared. Density ratings could then be averaged by layer and region for each case as well as across cases.

For illustrations, photomicrographs were acquired using a SPOT Insight 2.0 Mp color camera (Diagnostic Instruments Inc., Sterling Heights, MI). Camera exposure was set between 500 ms and 600 ms, and gain was set to 1. Photomicrographs were taken at 4x or 10x. For some illustrations, contrast was enhanced.

3.4.2 Retrograde tracers

Retrogradely labeled cells were plotted at a total magnification of 100x using a Nikon Optiphot-2 or a Nikon E600 coupled to a computerized data collection system (Neurolucida, MicroBrightfield, Inc., Burlington, VT). Fluorescently labeled cells were plotted for a 1:10 series of 30 µm sections. Closed contours were drawn around each layer of each frontal region analyzed. For each section, the area of the closed contours, area of the layers within the prefrontal regions, and the total number of labeled cells within closed contours (region, layer) were quantified by Neurolucida and exported to excel. Because we plotted cells for a 1:10 series of 30 µm coronal sections, we estimated total numbers of labeled cells by summing plotted cells across the 1:10 series and multiplying by 10.

Cell numbers were then normalized in the following way. For a dataset of 39 retrograde cases, we have now counted all cells for a 1:10 series of coronal sections in a collection of 70 brain regions including cortical (30), subcortical (36), and hippocampal (14) structures [3, 29, 31]. We chose to normalize to the total number of cells summed across all 70 structures for the 39 cases. For each case in the 39 case dataset, we first summed all plotted labeled cells using Neurolucida software (Microbrightfield, Inc.). Because cells were plotted for a 1:10 coronal series, we multiplied by 10 to obtain the estimate of the total labeled cells for each case. We then obtained the mean of that total, and calculated a correction factor for each case. The correction factor for each case was the total number of labeled cells for that case divided by the mean total cells of all 39 cases. For the cases analyzed for the present study, the number of cells counted in layers I-III, V, and VI for each area were multiplied by the correction factor for that case.

This approach to normalization is based on the assumption that injection sites of similar size and efficacy should result in similar numbers of labeled cells, overall, though the patterns of labeling may be different. For example, one region may receive a larger proportion of input from subcortical than cortical or hippocampal structures. Using our archival data eliminated effects of gross influences on individual cases, such as differences in injection size or quality, transport, quality of reagents, and survival time.

The volume of each afferent region was estimated by summing the areas of the regional contours and multiplying by 10 to account for the analysis of a 1 in 10 series and by 30 µm to account for the section thickness. Densities of labeled cells for each coronal section analyzed were calculated by dividing the total normalized number of labeled cells in each region by the volume of the region. We also calculated the densities for specific layers in the prefrontal regions. This was done by dividing the number of labeled cells within a layer by the volume of that layer. The percent of input arising from the afferent regions to a particular target structure was also calculated. The percentages were based on the normalized total number of labeled cells estimated for each prefrontal afferent region.

We assessed both densities of labeled cells and percentages of input because, although both are useful for assessing pattern and strengths of connections, they provide qualitatively different views of the impact of prefrontal afferents to the PER and POR. The density measure can be used to determine whether a particular prefrontal region projects more strongly to one target region than another. For example, does the MOs project more strongly to PER area 35 or to PER area 36? The percentage measure is more useful for evaluating the pattern of prefrontal inputs to a particular target region. For example, does the POR receive more input from ACAv than from ACAd? The percentage measure also allows comparison of the overall patterns of prefrontal input across target regions, for example by correlation analysis. To summarize, the density measure is more useful for assessing the strength and pattern of output from prefrontal

afferent regions, and the percentage measure is more useful for examining the relative strength and pattern of prefrontal input to the PER and POR.

4.0 Results

4.1. Description of Injection Sites

Ten injections of anterograde tracers were selected for analysis from a library of 29 (Table 1). Sites were chosen in order to span the rostral and caudal areas of PER and POR (Figure 1C, upper). The injection site was defined as the area that showed labeled cell bodies. We analyzed four sites in PER area 36, two sites in area 35, and four sites in the POR. Examples of fiber labeling are shown in Figure 3.

Nineteen injections of retrograde tracers were selected from a library of 72 retrograde tracer injection sites in the PER and POR (Table 2). The area of the injection site was defined as the dye core plus the region of heavy necrosis immediately surrounding the dye core. We analyzed nine sites in PER area 36, four sites in area 35, and six sites in the POR (Figure 1C, lower). Figure 4 shows retrogradely labeled cells from representative cases.

4.2. Prefrontal efferents of the PER and POR

Overall, PER area 36 projects most strongly to prefrontal areas IL and PL. The next strongest projections are to the orbitofrontal areas followed by MOs and ACAd. The weakest projections are to ACAv. The prefrontal projections arising in area 35 were similar except that the orbitofrontal efferents were slightly weaker and the MOS efferents were slightly stronger. For the POR, the strongest projections are to the MOs, ACAd, ORBvI, and ORBI. The weakest projections target the medial prefrontal areas, IL and PL. Overall, the prefrontal efferents of areas 36 and 35 are more similar to one another than to those of the POR.

4.2.1. PER efferents to prefrontal areas

Both area 36 and area 35 project to ORBI, ORBVI, and ORBm. The projection arising from area 36 is stronger than that arising from area 35 (Table 3). Injections in area 36 resulted in moderately dense fiber labeling (Figure 3A), whereas area 35 sites resulted in sparse labeling. Rostral and mid-rostrocaudal injection sites in both subdivisions produced more labeling than the most caudal sites. Overall, the resulting fiber labeling was heaviest at rostral levels of the orbital regions (Figure 5A, B). Thus, rostral and mid-rostrocaudal levels of the PER project to rostral levels of all three orbital regions. All anterograde injections sites in PER areas 36 and 35 resulted in labeled fibers in all layers, and labeling tended to be heaviest in layers I-II and V.

All levels of PER areas 35 and 36 project to the rostrocaudal extent of both IL and PL (Table 3). Overall, the strongest projection is from area 36 to PL and IL (Figure 3B, C). For area 36, the projection arising from midrostrocaudal sites was strongest, and the projection arising from caudal sites was weakest. The resulting fiber labeling was throughout rostrocaudal levels of IL and PL (Figure 5A). For area 35, the resulting fiber labeling in PL was strongest in midrostrocaudal levels regardless of where the projection originated (Figure 5B). Labeling in IL showed little evidence of topography. For areas 36 and 35, the labeled fibers were observed in all layers. In some cases, layer VI was sparsely labeled (Figure 3C-D).

All rostrocaudal levels of PER areas 36 and 35 project to anterior cingulate areas. Fiber labeling in ACAd was heavier that that observed in ACAv for both regions (Table 3 and Figure 3C). The projections arising from areas 36 and 35 are similar in terms of the topography of the projections. There was no obvious topography for ACAv labeling, but for ACAd the density of labeled fibers was heavier in the rostral two-thirds of the region (Figure 5A,B). In terms of the laminar patterns, labeling in ACAv was largely restricted to superficial layers, whereas labeling in ACAd was observed in laters II-V.

Both PER areas 36 and 35 project to MOs, though compared to other prefrontal efferents, the MOs projection is relatively weak (Table 3). Similar to the projections to ACAd, the

entire rostrocaudal extent of both PER areas 36 and 35 project to MOs. Unlike the anterior cingulate projection, however, there was some topography. Rostral areas 36 and 35 project preferentially to rostral MOs (Figure 5A, B). For both areas 36 and 35, the projections to MOs preferentially target layers I-III, especially layer I. Fiber labeling was less dense in layers V and VI.

4.2.2 POR efferents to prefrontal regions

Overall, the POR projections to frontal areas were weak compared with those arising in the PER. There were however, dramatic differences in the patterns of labeling arising in POR compared with PER. The strongest projections arising in the POR targeted ORBvI, ACAd, and MOs (Table 3). The density of labeling observed in ORBvI and superficial ORBI following POR injections was slightly heavier than that observed in ORBm (Figure 3G). Fiber labeling in the more caudal injection sites produced more labeling in all three orbital areas. For ORBI and ORBvI, fiber labeling was denser in rostral portions (Figure 5C). Labeling was most dense in superficial layers, especially layer I (Figure 3G).

The POR projections to both the IL and the PL are weak, but the projection to PL is very slightly stronger (Table 3). Fiber labeling in IL and PL resulted from injections in both rostral and caudal POR. For IL, fiber labeling was observed in rostrocaudal levels, but for PL, labeling was denser in rostral and caudal levels, but not weak in mid-rostrocaudal levels (Figure 5C). Labeling was primarily in superficial layers in the IL, but was in all layers of the PL.

POR projects to both anterior cingulate regions (Table 3). Overall the projection is fairly weak, but the projection to ACAd is stronger than the projection to ACAv (Figure 3H). POR projects to all rostrocaudal levels of both anterior cingulate areas (Figure 5C).

The entire rostrocaudal extent of POR projects to the MOs, but the projection arising from caudal POR is the strongest. The projection arising in caudal POR shows an interesting topography such that there are two peak areas of labeling. The pattern can be described as

heavier to the second and fourth quarters of the rostrocaudal extent of MOs (Figure 5C). The pattern is interesting because a rostral component of the MOs is proposed to be the rodent homolog of the primate DLPFC [25, 27]. Overall, labeling in the MOs following POR injections was strongest in superficial layers I-III, especially layer I (Figure 3I). Labeling was slightly weaker in layer V than layers II-III and was weakest in layer VI.

4.3. Prefrontal afferents of the PER and POR

Prefrontal afferents were analyzed by two measures: density of labeled cells in afferent regions (Table 4) and percentages of total input to target regions (Table 5). Each measure permits evaluation of the strength and pattern of prefrontal afferents to the PER and POR, but they provide different views of the impact of the afferents. The percentage measure allows the assessment of the overall pattern of prefrontal inputs to a particular target region. In other words, the density measure is more useful for assessing the strength and pattern of output from prefrontal afferent regions, whereas the percentage measure is more useful for assessing the relative strength and pattern of prefrontal input to target regions.

Table 5 also shows the normalized mean total numbers of labeled cells for each case. Thus the reader can calculate estimated total numbers of cell labeled in each region.

Numerically, PER area 35 injections yielded the most prefrontal labeled cells with (8,431±2878), followed by area 36 (5,127±1450) and then POR (5,191±869). As with the efferents, the patterns of afferent input to PER areas 36 and 35 were more similar to each other than to those of the POR.

4.3.1. Prefrontal afferents of the PER

The orbital regions provide stronger projections to PER area 35 than to area 36. This is evident in the higher densities of labeled cells for each of the ORB subdivisions (Table 4). ORBI provides nearly three times stronger projection to area 35 than to area 36. The ORBVI provides a stronger output to area 36 than ORBI and ORBm do. Whereas, ORBI provides the strongest

output to area 35, followed by ORBvI and then ORBm. For area 36 the strongest input arises from caudal ORBvI and all rostrocaudal levels of ORBm (Figure 5D). For area 35, the strongest input is from caudal ORBvI followed by all rostrocaudal levels of ORBI (Figure 5E). In terms of the relative strength of inputs, area 36 receives 47% of its total prefrontal input from orbitofrontal regions with the larger proportion arising from ORBvI (Table 5). For area 35, 37% of its total prefrontal input comes from orbitofrontal regions. The inputs from ORBI and ORBvI are nearly 2-4 times larger than those arising in ORBm. The projections arise largely in layers II-III (Figure 4A and 4D, areas 36 and 35 respectively).

The medial prefrontal regions project more strongly to PER area 35 than to area 36 (Table 4). For both area 36 and area 35, the IL is more densely labeled than the PL (Figure 4B and 4E, areas 36 and 35 respectively). Also for both target regions, the inputs are stronger from rostral levels of IL and PL than from caudal levels. In terms of the relative strength of inputs, area 36 receives 15% of its total prefrontal input from medial prefrontal regions with the larger proportion arising from PL (Table 5). For area 35, 8% of its total prefrontal input comes from medial prefrontal regions. The densities of labeled cells were highest in layers II-III followed by layer V and then layer VI (Table 4 and Figure 4B, E). Because layer V is larger in volume, a larger percentage of input arises in layer V (Table 5) even though the density of labeling is not the highest (Table 4).

The anterior cingulate regions project only weakly to areas 36 and 35, but the density of labeled cells is higher in ACAd than in ACAv for both target regions (Table 4). The ACAd projection to areas 36 and 35 arises from all rostrocaudal levels of the region, but the rostral parts may project slightly more strongly. Regarding the relative strength of inputs, for both areas 36 and 35, the input arising from ACAd is about 4% and 13% of the total, respectively, and the input from ACAv is negligible (Table 5). The ACAd projections to area 36 appear to arise mainly from layer V, whereas the area 35 input arises mainly from layers II-III (Figures 4C, F).

The MOs projection to PER areas 35 and 36 is roughly similar in strength to that of the prelimbic projection with higher densities of labeled cells following area 35 injections (Table 4). For area 36 there is a topography such that more rostral levels receive stronger inputs from the MOs than more caudal levels. In addition, the area 36 projections arise from a mid-rostrocaudal level and the most caudal level of MOs (Figure 5D). In terms of the relative strength of inputs, the inputs arising from the MOs account for the largest overall input for both areas, 34% for area 36 and 40% for area 35 (Table 5). For area 35, the projection also arises in rostral and caudal MOs, but more strongly from rostral MOs (Figure 5E). The projection terminates in all rostrocaudal levels of area 35. For both areas 36 and 35 the MOs projection arises largely in layers II-III and V (Figure 4C, F).

4.3.2. Prefrontal afferents of POR

Based on density of retrogradely labeled cells, ORBvI provides the strongest orbitofrontal projection to the POR, followed by ORBm (Table 4). ORBI provides the weakest projection. The ORBvI and ORBm projections arise in rostral levels, whereas the ORBI project arises in caudal levels (Figure 5F). The picture is slightly different based on percentages of input with ORBvI providing 36% and the other two areas providing 1-2% (Table 5). Labeled cells were observed primarily in layers II-III and V (Figure 4G). Negligible labeling was observed in layer VI.

Of all the frontal regions, the weakest projections arise in the medial prefrontal areas. The projection arising in PL is even weaker than that arising in IL (Table 4). In terms of the relative size on the inputs each region provides about 2% of the total input to the POR (Table 5), IL 3% and PL 0.1%. Interestingly, the laminar origin of the projections differed for IL and PL (Figure 4H). There is no evidence for any rostrocaudal topography of these projections. Moreover, the laminar origin of the projections differed for IL and PL (Figure 4H). The IL projection arises in layers II-VI, but the PL projection arises only in deep layers V and VI.

Both the ACAv and the ACAd project to the POR, but the projection from ACAd is about twice as strong based on densities of labeled cells (Table 4). As a proportion of total prefrontal input to the POR, the ACAd provides a much larger input accounting for 10% in contrast to only 1% arising from ACAv (Table 5). The ACAd projection arises in the caudal two-thirds of the region (Figure 5F). The projection targets all parts of the POR. Similar to the PL projection, the anterior cingulate projections arise in deep layers V and VI (Figure 4I).

The densities of labeled cells in the MOs are similar to that of IL and ACAv (Table 4). However, as a proportion of total prefrontal input to the POR, the MOs provides the largest input, accounting for 47% of the total prefrontal input to POR (Table 5). The MOs projection arises at two rostrocaudal levels, a mid-rostrocaudal level and the most caudal level. The projection terminates more strongly in rostral POR than in caudal POR. Interestingly, the projection arises mainly in layers II-V, with the largest density of labeled cells in layer V (Figure 41).

4.4. Summary of laminar patterns of connections

4.4.1. Prefrontal efferents of PER and POR

PER area 36 projects strongly to IL and PL. Labeling was strong in all layers, but in some cases, labeling in layer VI was weaker compared to that of layers I to V. The orbitofrontal cortices receive the next strongest projection. Labeling was strong in all layers but tended to be stronger in layers I-II and layer V than layer VI. Area 36 projects moderately to MOs. Projections preferentially targeted layers I-III. There was some labeling in layer V as well. Projections to the cingulate cortices are weaker. Labeling was stronger in the superficial layer for ACAv and in layers II-V for ACAd.

Compared to PER area 36, area 35 projects less strongly to the orbitofrontal cortices and slightly more strongly to MOs. Projections to the orbitofrontal cortices terminated in all

layers, but labeling was heavier in layers I-III. Projections to IL and PL were also very strong. Labeling was stronger in layers I-III and layer V. Projections to ACAd and ACAv resembled those of area 36. Projections were stronger to the superficial layers of ACAv and layers I-III and V of ACAd. Projections to the MOs were moderately strong. Labeling was denser in layers I-III, especially layer I. Labeling was less dense in layer V and even more sparse in layer VI.

POR projections to the prefrontal cortices were, in general, weaker compared to those of the PER. Projections to the MOs and ACAd were stronger than the other prefrontal projections. The MOs projection preferentially target the superficial layers I-III, especially layer I. Labeling was weaker in the deeper layers, especially layer VI. Labeling in ACAd was strongest in layers I-III followed by layer V. Labeling in ACAv was very sparse in all layers. Projections to the orbitofrontal cortices were weak. Though sparse, labeling was stronger in the superficial layers of the orbitofrontal cortices. Projections to IL and PL was also weak. Very sparse labeling was observed in all layers of PL and in the superficial layers of IL.

4.4.2. Prefrontal afferents of PER and POR

Based on densities of labeled cells, prefrontal regions project more strongly to PER area 35, followed by area 36, and then POR (Table 4). The exceptions are ACAv and ACAd, which project more strongly to the POR than to either subregion of the PER as well asl MOs and ORBvI, which project more strongly to the POR than to PER area 36. In general, the projections tend to arise primarily from layers II-III followed by layer V.

Prefrontal projections to area 35 are strongest from the orbitofrontal cortices, especially to ORBI and ORBVI. Projections from the orbitofrontal cortices are stronger in layers II-III but also somewhat strong from the deeper layers, especially for ORBVI. Projections from the medial prefrontal regions are also strong, with the IL providing a stronger input than the PL. Projections arise largely in layers II-III for IL and from all layers of PL. The MOs provides the next strongest input to area 35 based on densities of labeled cells. The projection comes from all layers but is

strongest from layers II-III. Projections from ACAd are moderate arising mostly from layers II-III. The projection from ACAv is very weak. Based on percentages of input, the largest input arises in MOs, which is also the largest afferent region by volume. This is followed by ORBI and then ORBvI.

PER area 36 receives its strongest input from layers II-III of orbitofrontal cortices. The next strongest inputs originate from the medial prefrontal areas of IL and PL. The projection from the IL is stronger than that of the PL and originates primarily from layers II-III where cells are more densely labeled. The projection from the PL arises in layers II-III and V. The MOs provides moderate size input to area 36, arising largely from layers II-III and V. The anterior cingulate regions' projections to area 36 are weak, especially from ACAv. The projection from ACAd arises mainly in layer V followed by layer II-III. Again, based on percentages of input, the MOs provides the largest proportion of prefrontal input to area 36.

The strongest prefrontal input to the POR based on densities of labeled originates in layers II-III of ORBvI followed by layer V. Input is moderate from layers II-II of ORBm and negligent from ORBI. Projection from the ACAd is also strong and that from ACAv is moderately strong. Interestingly, these projections arise in deep layers V and VI. Input from the MOs is also moderately strong and arising primarily in layer V. Medial prefrontal input is weaker, especially from PL. Based on percentages, MOs accounts for 47% of the total input to the POR followed by ORBvI, which accounts for 36%.

5. Discussion

5.1. Summary of findings

In the present study, we investigated the PFC connections with the PER and the POR using descriptive and quantitative anterograde and retrograde tract tracing methods.

Importantly, our analyses included an evaluation of the topographical and laminar patterns of labeling. For the retrograde analyses, the total numbers of retrogradely labeled cells per case

were normalized to a large dataset consisting of 39 neuroanatomical cases in which labeled cells were quantified in a total of 70 neocortical, parahippocampal, hippocampal, and subcortical structures [3, 29, 31, 39]. In Burwell and Amaral [3] it was necessary to normalize to manual counts for 30 cortical regions because those were the available data at the time. In Tomas Pereira et al. [31] we normalized in a fashion similar to that used in the present study because we had available automated counts for all cortical, subcortical, and hippocampal structures. For the anterograde analyses, we normalized across cases by identifying the strongest and weakest labeling for each case and then assigning these densities of labeled fibers as very dense and very sparse, respectively, as we have done in prior studies [28]. These approaches to normalization control for both unknown and known differences across cases. Of course, even the most accurate estimate of retrogradely labeled cell numbers or densities of labeled fibers in a particular prefrontal region does not fully account for differences in strengths of connectivity. Cases selected for analysis may not be representative, and the strength of synaptic contacts is not accounted for. Nevertheless, such quantitative data are valuable and can inform other studies, for example circuit analysis studies or studies of synaptic connectivity.

Prefrontal efferents to the PER and POR appear to differ in overall strength. We found that tracer injections located in the PER resulted in significantly more labeled fibers than tracer injections located in the POR (Figure 6A). The patterns of labeling also differed across regions. Area 36 projects most strongly to PL and IL followed the orbitofrontal projections. Area 35 shows a similar pattern, though the projections to the orbitofrontal regions are not as strong as those arising in area 36. POR projects weakly overall, but its strongest projections are to ACAd, ORBvl. and MOs.

The prefrontal afferents to the PER and POR seem to be roughly similar in terms of the overall size of the prefrontal input as indicated by the mean total and standard error of normalized numbers of labeled cells in PER area 36 (5127±1450), area 35 (8431±2878), and

the POR (5191±869) shown at the bottom of Table 5. The similarities in overall size of prefrontal input is also evident in Figure 6B. Comparison of panels A and B of Figure 6 shows that the prefrontal projections to the PER and are largely reciprocated with regard to targets, but not necessarily in strength as represented by densities of labeled cells. For example, whereas area 35 projects more strongly to medial prefrontal than orbitofrontal areas (Figure 6A), the reciprocal projection is stronger from orbitofrontal than from medial frontal regions (Figure 6B).

The differences in the patterns of inputs to each of the three regions are perhaps easiest to comprehend when examining the percentages of total input (Figure 6C). The complement of inputs differs for area 36, area 35, and POR, though the inputs to areas 36 and 35 area more similar to each other. PER area 36 receives its largest input from orbitofrontal regions, which accounts for a total of 46%, followed by 34% from MOs and 15% from medial prefrontal areas. Area 35 receives its largest input from MOs (40%), followed by orbitofrontal regions 37%), and then ACAd (13%). Input to the POR was dominated by the MOs (47%) and ORBvI (36%) with the only other sizeable input arising in ACAd (10%).

Interestingly, all three target regions receive a substantial input from the MOs and these connections are reciprocal. There are similarities in the topography of these connections (Figure 5). For area 35 the connections with rostral MOs are stronger than the connections with caudal MOs. For the POR, the strongest efferents originate in two locations, rostral to mid-rostrocaudal MOs and in caudal MOs. POR projections to the MOs show a similar pattern. For area 36, the projection to the MOs is similar to that of area 35 and preferentially targets rostral MOs. The input from MOs is similar to that of the POR with inputs arising largely from two locations, rostral to mid-rostrocaudal MOs and the caudal MO.

4.2 Comparisons with prior studies

A number of studies have used tract tracing methods to examine the anatomical connectivity between the rodent PFC and the PER and POR. The present study comprises

more detailed and/or quantitative analyses of the prefrontal component of data that were previously published [3, 28]. Here, we provide more detail regarding the laminar patterns and the topography of the connections. With regard to the efferents, the present analysis is consistent with what we reported for overall strength of projections with a few minor exceptions. Here, we find the MOs projection to POR, and the medial prefrontal projections to area 35 slightly stronger than we previously reported. Overall, the patterns of labeling were similar across the two studies. For percentages of total labeled cells, the patterns across the two studies were significantly correlated with r values of 0.96, 0.95, and 0.87 for area 36, area 35, and POR, respectively. For densities of labeled cells, the patterns were also significantly correlated across the two studies as indicated by r values of 0.94, 0.99, and 0.96 for area 36, area 35, and POR, respectively. Thus, the *relative* sizes of inputs to the PER and POR are similar across the two studies.

With regard to the prefrontal afferents, the densities and total numbers of cells were higher in the current study than in our prior study [3], especially for area 35. This is because in the earlier study areal volumes were likely overestimated and cell numbers underestimated resulting in lower densities of labeled cells. This can be accounted for by differences between the two studies in how data were acquired and normalized. In the earlier study, we used the fractionator method in which a fraction of the volume of the structure is sampled and used to estimate total volumes and numbers of cells. The sampled cells were then multiplied by the reciprocal of the fractional volume to obtain an estimate of the number of cells. Only a fraction of the structure in each coronal section was sampled. In addition, cells in sample fractions were manually counted from printouts of the digital data. This resulted in under sampling in regions in which cells were most densely labeled, as plotted cells could and often did obscure one another. In the present study, identified labeled cells were counted for the entire area of a target region, rather than a fraction of the area, in one of every 10 coronal sections. In addition, counting of plotted labeled cells was automated using Neurolucida software. Thus in the

present study, we assessed a much larger fraction of the volume, and we were able to more accurately count labeled cells. Another difference between the present study and Burwell and Amaral [3] is that the current data are normalized to total cell numbers counted in cortical, hippocampal, and subcortical regions, whereas the earlier numbers were normalized only to numbers of labeled cells counted in cortical regions. At the time the earlier paper was written, we had not yet quantified the subcortical and hippocampal connections, so the only data available for normalization across cases were the fractionator data for cortical regions. For the present study we had automated cell counts for all cortical, subcortical and hippocampal regions available for normalization across cases.

Our efferent findings should also be compared with those of Delatour and Witter [43], who also used anterograde tracers to study the prefrontal efferents of the PER and POR. They included insular cortex, but not MOs, and we included MOs, but not anterior insular cortex. The results reported by Delatour and Witter for the POR are similar to our findings with the exception that they did not mention labeling in anterior cingulate cortex, whereas we found dense fiber labeling in layers I-III and V of ACAd. There are more differences between the findings of the two studies with respect to the prefrontal efferents of the PER. Both studies reported massive projections to PL and IL, terminating in superficial layers. We also observed labeling in layer V. Delatour and Witter reported that medial prefrontal labeling emerged from rostral PER and that labeling in the PL was stronger in rostral levels than caudal levels. We found that area 36 targeted rostral levels of the IL and PL most strongly and that the strongest input emerged from midrostrocaudal levels of area 36. In contrast, the area 35 projections emerged from rostral and caudal levels and preferentially targeted midrostrocaudal levels of PL and all levels of IL. With regard to orbital regions, Delatour and Witter reported weak to moderate labeling in superficial layers. We found moderate to strong labeling in all layers. In addition, for both area 35 and area 36 the orbital projections tended to emerge from rostral PER and terminate in rostral orbital regions. The projection from area 36 was stronger to ORBI and ORBm.

Whereas the findings of the present study and those of Delatour and Witter [43] are generally consistent, we found stronger labeling in orbital regions and a more complicated topography of the projections. One major difference between the two studies is that we analyzed PER areas 35 and 36 separately. This may account for the differences in topography. Two other differences between the two studies are 1) survival time was longer for some of our cases, and 2) we normalized labeling for each case. These differences may account for our findings of stronger labeling in orbital regions.

Delatour and Witter [43] suggested that parahippocampal projections to prefrontal areas form two pathways. One emerges from PER and lateral entorhinal areas and targets mainly medial prefrontal regions. The other emerges from POR and targets mainly ORBvI. Our data are consistent with that view with the exception that we find the POR projections to ACAd and MOs to be as strong as the ORBvI projection. We also find that PER projections to orbitofrontal regions are stronger than those arising in the POR and are nearly as strong as PER projections that target IL and PL.

Jones and Witter [44] reported that the medial prefrontal and cingulate cortices project extensively to PER and POR. They reported that IL, PL, the rostral two-thirds of ACAd, and the rostral half of ACAv project to PER, whereas the caudal two-thirds of ACAd and all of ACAv preferentially target the POR. These findings are largely consistent with our own. For example, the relative sizes of the projections are consistent across the two studies. Because the present study employed retrograde methods and Jones and Witter [44] used anterograde methods, the two studies are complementary and together give a full picture of the laminar patterns of the origins and terminations of these projections. To summarize, the IL projection to PER arises preferentially in layers II-III, but also from layer V and to a lesser extent in layer VI. The projection terminates preferentially in superficial layers and to a lesser extent in deep layers.

a lesser extent in superficial layers. The ACAd projection to POR arises in layers V-VI and terminates preferentially in deep layers, although, a smaller projection arising in superficial layers of ACAd may target all layers of the POR. The ACAv projection to POR also arises in layers V-VI and terminates preferentially in deep layers.

Regarding prefrontal afferents, our findings for orbital inputs to the PER and POR are largely consistent with those of Kondo and Witter [45]. We analyzed PER areas 35 and 36 separately and we also included ventral ORB with ORBvl. Kondo and Witter reported that the strong projection to the POR arises in ventral ORB rather than ORBvl. An examination of our material indicated that the strongest labeling was in the medial portion of ORBvl, which corresponds to ventral ORB. Again our study combined with that of Kondo and Witter [45] allows the possibility to extract the laminar origins and terminations of the ORB projections to the PER and POR. For example, we find that the ORB projections to PER and POR arise preferentially in layers II-III and to a lesser extent in layers V-VI. Kondo and Witter [45] reported that the POR projection terminates mainly in superficial layers.

5.2. Functional implications

One rationale for the present study was to better understand the functional connectivity of the MOs. Interestingly, PER areas 36 and 35 as well as the POR are strongly interconnected with MOs exhibiting two topographies. PER area 36 efferents and POR efferents and afferents exhibit a bimodal topography such that one set of connections involves rostral to midrostrocaudal MOs and the other involves caudal MOs. This is interesting because the rostral component of MOs may be the homolog of the primate DLPFC, which comprises Brodman's area 46 [25]. This putative homology is supported by our finding that labeled cells in the MOs accounted for nearly half of all labeled cells in prefrontal areas resulting from POR injections. Similarly, the primate PHC receives strong input from DLPFC [46]. Like the primate DLPFC, the rodent MOs receives input from sensory areas and projects to motor-related regions [47-49]. In

addition, it was suggested that the caudal extent of MOs shows homology with primate frontal eye fields [27].

Wise [19] argued that the most rostral components of the primate prefrontal cortex, which include DLPFC, do have not homologs in the rodent brain. Those arguments, however, did not take into account connectional evidence or other features important for establishing homology in the nervous system [50]. Moreover for our purposes, there was little discussion of MOs (FR2 in Wise [19]). The primary claim of Wise [19] was that these forward regions confer an adaptive advantage by allowing the primate brain to integrate and evaluate information about contexts and outcomes especially in unusual or infrequent situations. We appreciate that assertions of prefrontal homology across primates and rodents should be made with caution, especially given the expansion of prefrontal regions in the primate brain. However, although it may be the case that entirely new and different brain regions appeared in the primate brain, we argue it is more likely that prefrontal regions already existing in the rodent brain expanded and became more highly differentiated with evolution. If that is the case, then the functional rudiments of the most rostral components of the primate brain should exist in the rodent brain. These functional rudiments are also important for establishing homology.

Functional evidence that the rodent MOs may be the homolog of the primate DLPFC is available. A review of the literature suggests that rostral ACAd and MOs are functionally, as well as connectionally, similar to the primate ventral DLPFC [20]. This review, which focused on visuospatial working memory in monkeys and rats, covered anatomical, neuropsychological, and electrophysiological studies in both species. A relevant finding of multiple studies is that the both the primate vDLPFC and the rodent ACAd/MOs code information including cue location and response direction in sustained delay activity. Lesion studies of the non-human primate DLPFC show that the region has an important role in visuospatial control of actions and is heavily connected with premotor cortex and posterior parietal cortex [reviewed in 51]. In rodents, lesions to the MOs are known to impair exhibition of motor response to sensory input,

without disturbing sensory perception, action initiation, or performance [26, 52, 53]. The MOs is also necessary for processing goal-directed decisions dependent on sensory information and reward [54]. Thus, like PHC and DLPFC in primates, the POR, ACAd, and MOs in rats may be part of a network that is important for visual attention and working memory for spatial position.

Earlier studies provide evidence for multiple pathways between parahippocampal and prefrontal regions. Kondo et al. [55] reported that the PER in monkeys is reciprocally connected with orbital prefrontal areas, whereas PHC is reciprocally connected with the medial prefrontal areas including area 9 and area 46. Delatour and Witter [43] reported that PER projects primarily to PL and IL and that the POR projects primarily to superficial layers of ORBvI. Our findings exhibit similiarities with both the monkey and the rat study. We did find that PER projects more strongly to medial prefrontal areas than to orbital prefrontal areas, but both sets of projections are massive. We also found that POR projects more strongly to ORBvI than to other orbital regions or to the ventral medial prefrontal regions (IL and PL). However, the strongest prefrontal efferents emerging in POR target ACAd and MOs, supporting the case for homology with the primate DLPFC. Thus, we can say that our findings are consistent with those of [55], although these pathways in the monkey appear to be more highly differentiated than they are in the rat.

6. Conclusion

We have undertaken a comprehensive anatomical study of the prefrontal efferents and afferents of PER areas 35 and 36 and the POR, including the laminar and topographical patterns of these connections. Our inclusion of MOs and the anterior cingulate regions provided additional evidence that these regions provide a homolog to lateral and dorsolateral prefrontal cortex in the primate brain. As a consequence, our findings improve the use of rodent models for the study of human prefrontal and executive functions. Our hope is that the detailed analysis

of these connections will inform future studies of how PFC, PER, and POR areas interact in functional networks in the control of memory and attention.

Acknowledgements: The authors wish to acknowledge Devon Poeta for her assistance and training on microscopy, data collection, illustration, and data analyses.

Funding: This work was supported by the National Institutes of Health [R01MH108729] and the National Science Foundation [IOS-1656488].

7.0 References

- [1] R.D. Burwell, The parahippocampal region: corticocortical connectivity, Annals of the New York Academy of Sciences 911 (2002) 25-42.
- [2] R.D. Burwell, Witter, M. P., & Amaral, D. G., Perirhinal and postrhinal cortices of the rat: a review of the neuroanatomical literature and comparison with findings from the monkey brain., Hippocampus 5(5) (1995) 390-408.
- [3] R.D. Burwell, & Amaral, D. G., Cortical afferents of the perirhinal, postrhinal, and entorhinal cortices of the rat, Journal of Compartive Neurology 398(2) (1998) 179-205.
- [4] W.A. Suzuki, D.G. Amaral, Perirhinal and parahippocampal cortices of the macaque monkey: cortical afferents, J Comp Neurol 350(4) (1994) 497-533.
- [5] H. Eichenbaum, A cortical-hippocampal system for declarative memory, Nat Rev Neurosci 1(1) (2000) 41-50.
- [6] V.R. Heimer-McGinn, D.L. Poeta, K. Aghi, M. Udawatta, R.D. Burwell, Disconnection of the Perirhinal and Postrhinal Cortices Impairs Recognition of Objects in Context But Not Contextual Fear Conditioning, The Journal of neuroscience: the official journal of the Society for Neuroscience 37(18) (2017) 4819-4829.
- [7] F. Barthas, A.C. Kwan, Secondary Motor Cortex: Where 'Sensory' Meets 'Motor' in the Rodent Frontal Cortex, Trends in neurosciences (2016).
- [8] M.L. Dixon, K. Christoff, The lateral prefrontal cortex and complex value-based learning and decision making, Neuroscience and biobehavioral reviews 45 (2014) 9-18.
- [9] M.V. Puig, E.G. Antzoulatos, E.K. Miller, Prefrontal dopamine in associative learning and memory, Neuroscience 282 (2014) 217-29.
- [10] M. Rangel-Gomez, M. Meeter, Neurotransmitters and Novelty: A Systematic Review, Journal of psychopharmacology 30(1) (2016) 3-12.
- [11] M. Watanabe, M. Sakagami, Integration of cognitive and motivational context information in the primate prefrontal cortex, Cereb Cortex 17 Suppl 1 (2007) i101-9.

- [12] S.A. Beaudin, Singh, T., Agster, K. L., & Burwell, R. D, Borders and comparative cytoarchitecture of the perirhinal and postrhinal cortices in an F1 hybrid mouse, Cereb Cortex 23(2) (2013) 460-476.
- [13] R.D. Burwell, Borders and cytoarchitecture of the perirhinal and postrhinal cortices in the rat, Journal of Comparative Neurology 437(1) (2001) 17-41.
- [14] E. Franko, A.M. Insausti, E. Artacho-Perula, R. Insausti, C. Chavoix, Identification of the Human Medial Temporal Lobe Regions on Magnetic Resonance Images, Hum Brain Mapp 35(1) (2014) 248-256.
- [15] W.A. Suzuki, & Amaral, D.G., Perirhinal and parahippocampal cortices of the macaque monkey: Cytoarchitectonic and chemoarchitectonic organization, Journal of Comparative Neurology 463(1) (2003) 67-91.
- [16] S.R. Heilbronner, J. Rodriguez-Romaguera, G.J. Quirk, H.J. Groenewegen, S.N. Haber, Circuit based cortico-striatal homologies between rat and primate, Biological Psychiatry (2016).
- [17] D. Ongur, J.L. Price, The organization of networks within the orbital and medial prefrontal cortex of rats, monkeys and humans, Cereb Cortex 10(3) (2000) 206-219.
- [18] J.K. Seamans, Lapish, C.C., & Durstewitz, D., Comparing the prefrontal cortex of rats and primates: insights from electrophysiology, Neurotox Res 14(23) (2008) 249-262.
- [19] S.P. Wise, Forward frontal fields: phylogeny and fundamental function, Trends in neurosciences 31(12) (2008) 599-608.
- [20] K.I. Tsutsui, K. Oyama, S. Nakamura, T. lijima, Comparative Overview of Visuospatial Working Memory in Monkeys and Rats, Front Syst Neurosci 10 (2016) 99.
- [21] M. Petrides, Lateral prefrontal cortex: architectonic and functional organization, Philosophical transactions of the Royal Society of London. Series B, Biological sciences 360(1456) (2005) 781-95.
- [22] J.H. Sul, S. Jo, D. Lee, M.W. Jung, Role of rodent secondary motor cortex in value-based action selection, Nature neuroscience 14(9) (2011) 1202-8.

- [23] J.C. Erlich, M. Bialek, C.D. Brody, A cortical substrate for memory-guided orienting in the rat, Neuron 72(2) (2011) 330-43.
- [24] R. Kawai, Markman, T., Poddar, R., Ko, R., Fantana, A.L., Dhawale, A.K., Kampff, A.R., & Olveczky, B.P., Motor cortex is required for learning but not for executing a motor skill., Neuron 86(3) (2015) 800-812.
- [25] H.B. Uylings, C.G. van Eden, Qualitative and quantitative comparison of the prefrontal cortex in rat and in primates, including humans, Progress in brain research 85 (1990) 31-62.
- [26] R.P. Kesner, Subregional analysis of mnemonic functions of the prefrontal cortex in the rat, Psychobiology 28(2) (2000) 219-228.
- [27] H.B.M. Uylings, H.J. Groenewegen, B. Kolb, Do rats have a prefrontal cortex?, Behav Brain Res 146(1-2) (2003) 3-17.
- [28] K.L. Agster, & Burwell, R. D, Cortical efferents of the perirhinal, postrhinal, and entorhinal cortices of the rat, Hippocampus 19 (2009) 1159-1186.
- [29] K.L. Agster, & Burwell, R. D, Hippocampal afferents and efferents of the perirhinal, postrhinal, and entorhinal cortices, Behav Brain Res 254 (2013) 50-64.
- [30] K.L. Agster, I.T. Pereira, M.P. Saddoris, R.D. Burwell, Subcortical connections of the perirhinal, postrhinal, and entorhinal cortices of the rat. II. efferents, Hippocampus 26(9) (2016) 1213-1230.
- [31] I. Tomas Pereira, K.L. Agster, R.D. Burwell, Subcortical connections of the perirhinal, postrhinal, and entorhinal cortices of the rat. I. afferents, Hippocampus 26(9) (2016) 1189-212. [32] L.W. Swanson, Brain maps III: structure of the rat brain: an atlas with printed and electronic templates for data, models, and schematics, 3rd rev. ed., Elsevier, Academic Press, Amsterdam; Boston, 2004.
- [33] J.E. Krettek, J.L. Price, The cortical projections of the mediodorsal nucleus and adjacent thalamic nuclei in the rat, J.Comp.Neurol. 171 (1977) 157-192.

- [34] J.P. Donoghue, S.P. Wise, The motor cortex of the rat: Cytoarchitecture and microstimulation mapping, J. Comp. Neurol. 212 (1982) 76-88.
- [35] R.M. Beckstead, Convergent thalamic and mesencephalic projections to the anterior medial cortex in the rat, J.Comp.Neurol. 166 (1976) 403-416.
- [36] J.P. Ray, J.L. Price, The organization of the thalamocortical connections of the mediodorsal thalamic nucleus in the rat, related to the ventral forebrain-prefrontal cortex topography, J Comp Neurol 323(2) (1992) 167-97.
- [37] K. Brodmann, Vergleichende Lokalisationslehre der Grosshirnrinde in ihren Prinzipien dargestellt auf Grund des Zellenbaues, Barth, Liepzig, 1909.
- [38] G. Paxinos, C. Watson, Paxinos and Watson's the rat brain in stereotaxic coordinates, Seventh edition. ed.2014.
- [39] R.D. Burwell, & Amaral, D. G., Perirhinal and postrhinal cortices of the rat: interconnectivity and connections with the entorhinal cortex, Journal of Compartive Neurology 119(2) (1998) 293-321.
- [40] I.T. Pereira, K.L. Agster, R.D. Burwell, Subcortical connections of the perirhinal, postrhinal, and entorhinal cortices of the rat. I. afferents, Hippocampus 26(9) (2016) 1189-1212.
- [41] E. Dobo, V.T. Takacs, A.I. Gulyas, G. Nyiri, A. Mihaly, T.F. Freund, New silver-gold intensification method of diaminobenzidine for double-labeling immunoelectron microscopy, J Histochem Cytochem 59(3) (2011) 258-69.
- [42] D.A. Lewis, M.J. Campbell, J.H. Morrison, An immunohistochemical characterization of somatostatin-28 and somatostatin-281-12 in monkey prefrontal cortex, J Comp Neurol 248(1) (1986) 1-18.
- [43] B. Delatour, & Witter, M.P., Projections from the parahippocampal region to the prefrontal cortex in the rat: evidence of multiple pathways, European Journal of Neuroscience 15(8) (2002) 1400-1407.

- [44] B.F. Jones, M.P. Witter, Cingulate cortex projections to the parahippocampal region and hippocampal formation in the rat, Hippocampus 17(10) (2007) 957-76.
- [45] H. Kondo, M.P. Witter, Topographic organization of orbitofrontal projections to the parahippocampal region in rats, J Comp Neurol 522(4) (2014) 772-93.
- [46] K.S. Saleem, B. Miller, J.L. Price, Subdivisions and Connectional Networks of the Lateral Prefrontal Cortex in the Macaque Monkey, Journal of Comparative Neurology 522(7) (2014) 1641-1690.
- [47] F. Conde, Maire-Lepoivre, E., Audinat, E., & Crepel, F., Afferent connections of the medial frontal cortex of the rat. II. Cortical and subcortical afferents, Journal of Comparative Neurology 352 (1995) 567-593.
- [48] W.B. Hoover, & Vertes, R.P., Projections of the medial orbital and ventral orbital cortex in the rat., Journal of Comparative Neurology 519(18) (2011) 3766-3801.
- [49] R.L. Reep, Corwin, J. V., Hashimoto, A., & Watson, R. T., Efferent connections of the rostral portion of medial agranular cortex in rats, Brain Res. Bull. 19 (1987) 203-221.
- [50] C.B. Campbell, W. Hodos, The concept of homology and the evolution of the nervous system, Brain Behav Evol 3(5) (1970) 353-67.
- [51] E.M. Aminoff, K. Kveraga, M. Bar, The role of the parahippocampal cortex in cognition, Trends Cogn Sci 17(8) (2013) 379-90.
- [52] A. Cowey, Bozek, T., Contralateral "neglect" after unilateral dorsomedial prefrontal lesions in rats., Brain Res. 72 (1974) 53-63.
- [53] D.P. Crowne, Pathria, M.N., Some attentional effects of unilateral frontal lesions in the rat., Behav. Brain Res. 6 (1982) 25-39.
- [54] J. Sul, Jo, S., Lee, D., & Jung, M., Role of rodent secondary motor cortex in value-based action selection, Nature neuroscience 14 (2011) 1202-1208.

[55] H. Kondo, K.S. Saleem, J.L. Price, Differential connections of the perirhinal and parahippocampal cortex with the orbital and medial prefrontal networks in macaque monkeys, J Comp Neurol 493 (2005) 479-509.

Figures C Α POR **POR PER PER** 129B 39P 83B 36 54P 36 rs 35 16P rs 24P **POR** В **PER** MOs 132DY 120DY ACAd 99FB 94FB 100D 02FB AČAv 95DY \ 98FB ORBm 98DY 36 99DY **√**97DY 112DY 108FG rs 35 102DY 132FB 1 mm

Figure 1. Anatomical areas under investigation. A. Surface view of the of the rat brain showing the location of the perirhinal cortex (PER) and postrhinal cortex. B. Midsagittal view of the rat brain showing the locations of the frontal regions under investigation. These include secondary motor cortex (MOs), dorsal anterior cingulate cortex (ACAv), prelimbic cortex (PL), infralimbic cortex (IL), medial orbital cortex (ORBm), ventral orbital cortex (ORBv), and ventrolateral orbital cortex (ORBvI). C. Unfolded map showing the locations of anterograde injection sites (upper) and retrograde injection sites (lower). Injections that involved only deep layers are shown in dark grey and only superficial layers are in light grey. Injections shown in middle grey involve all layers. Each injection site is labeled with the case name. Other abbreviations: C, caudal; D, dorsal; R, rostral; V, ventral; rs, rhinal sulcus.

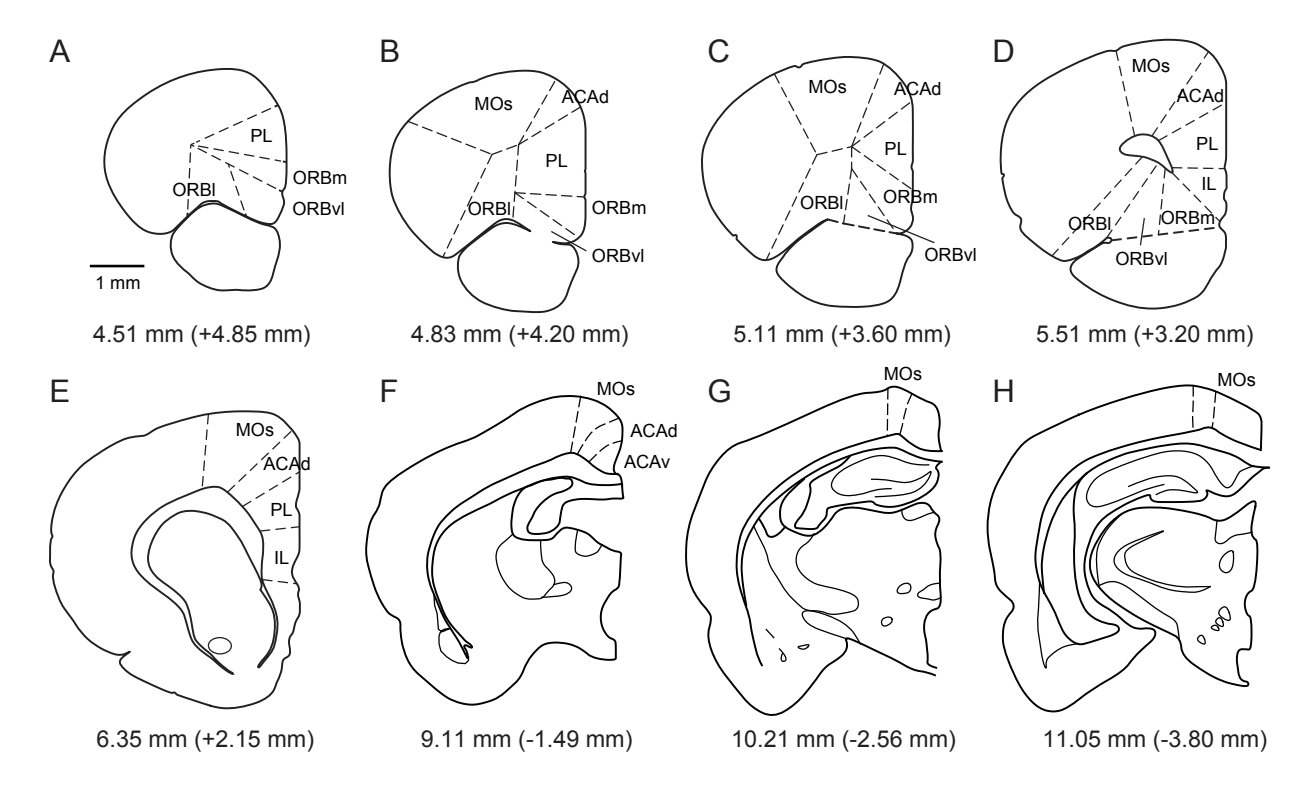


Figure 2. Cortical boundaries for all frontal regions quantified for a subset of coronal sections of a representative rat brain. Regions analyzed includes secondary motor cortex (MOs), dorsal anterior cingulate cortex (ACAd), ventral anterior cingulate cortex (ACAv), prelimbic cortex (PL), infralimbic cortex (IL), medial orbital cortex (ORBm), ventral orbital cortex (ORBv), and ventrolateral orbital cortex (ORBvl). The first number below each section is the absolute rostrocaudal plane of the section (Swanson, 1992). The second is relative to bregma.

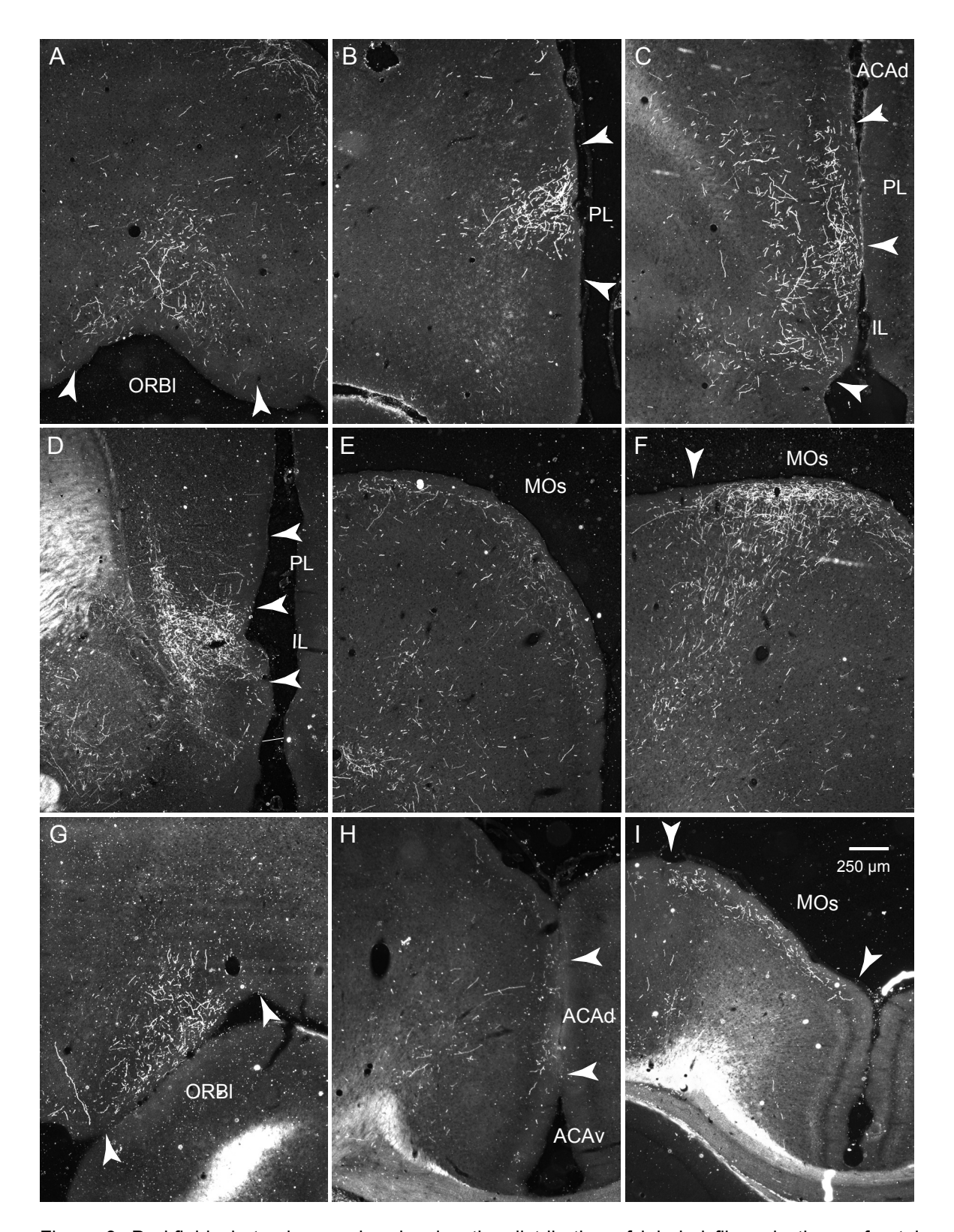


Figure 3. Darkfield photomicrographs showing the distribution of labeled fibers in the prefrontal regions. Panels A-C, E, and F. Labeled fibers from tracer injections in PER area 36 at coronal levels of +5.2, +3.2, +4.8, +4.8, and +3.6 mm relative to bregma. D. Labeled fibers from a site in area 35 shown at level +2.7 mm. G-I. Labeled fibers from sites in POR at levels of +4.6, and +0.5, and -0.5 mm. Scale bar = 250 μ m.

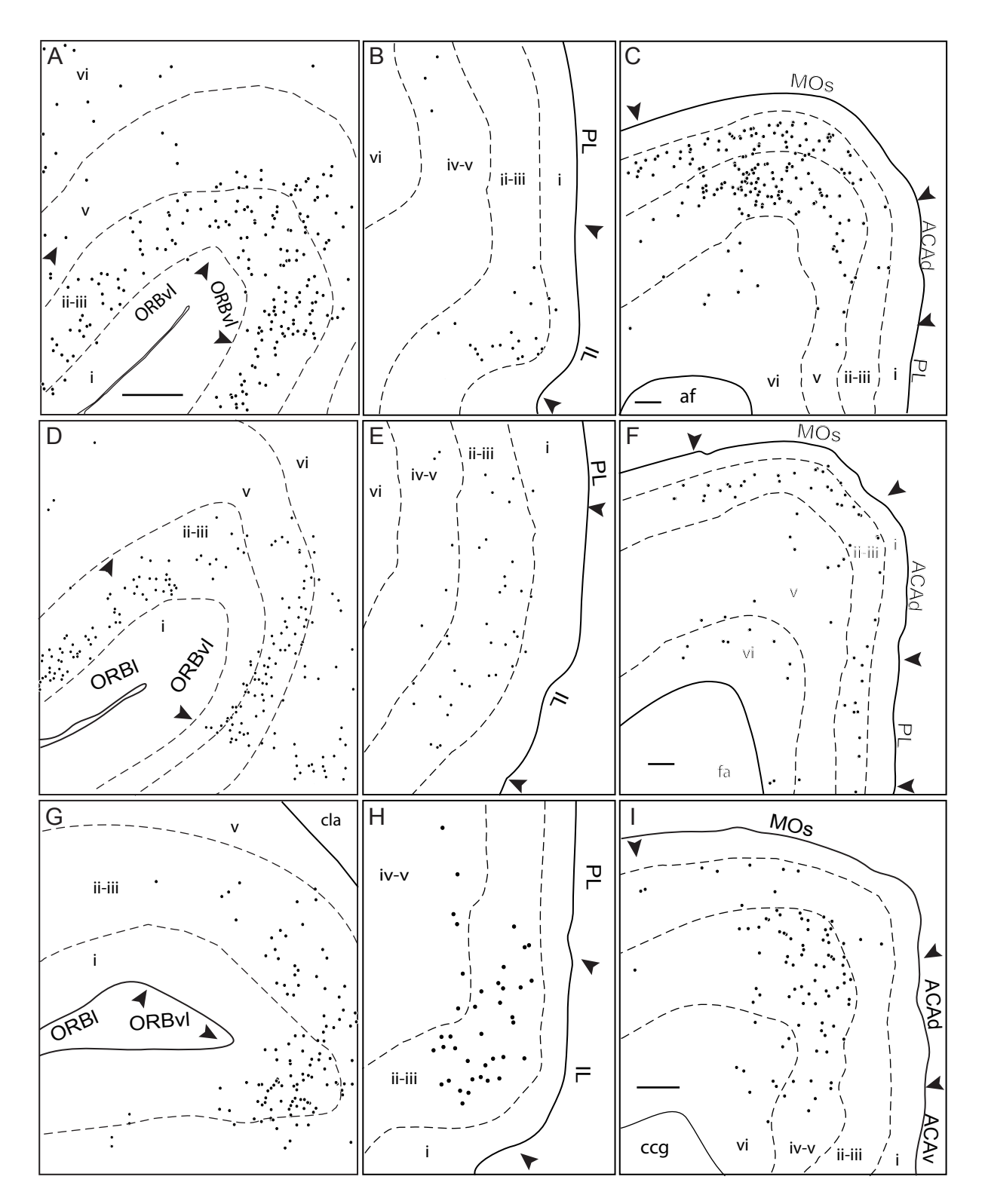


Figure 4. Regional and laminar contours with retrogradely labeled cells in prefrontal regions arising from tracer injections in PER and POR. A-C. Labeled cells from injection sites in PER area 36 shown at coronal level +3.2, +2.8, and +3.2 mm relative to bregma. D-F. Labeled cells from sites in area 35 shown at coronal levels +3.3, +3.2, and +2.8. G-I. Labeled cells arising from sites in POR shown at coronal levels +3.6, and +2.8 mm. Scale bar = $250 \mu m$. Panels B, D, E, G, and H are on the same scale as panel A. Other abbreviations: corpus callosum anterior forceps, fa; corpus callosum genu, ccg.

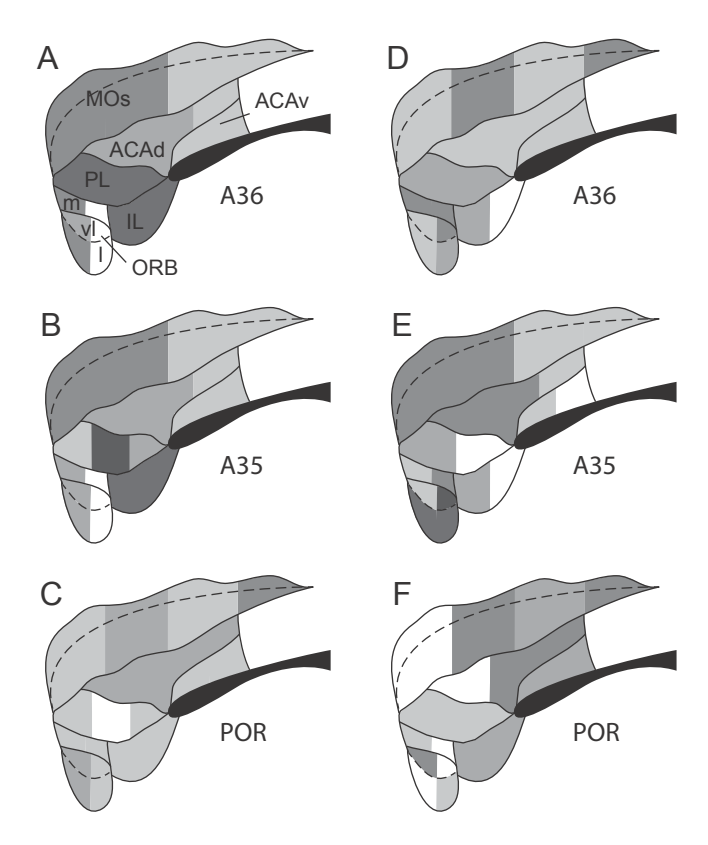


Figure 5. Flatmaps of prefrontal regions showing the pattern of labeling for PER and POR efferents and afferents. A-C. Patterns of anterograde labeling arising from injections in PER area 36 (A), area 35 (B), and POR (C). Frontal regions are indicated in the upper panel. D-F. Patterns of retrograde labeling arising from injections in PER area 36 (D), area 35 (E), and POR (F). White indicates zero or negligible labeling. Five levels of gray range from very light (sparse labeling) to dark grey (very dense labeling). The corpus callosum is shown in black. See text for abbreviations.

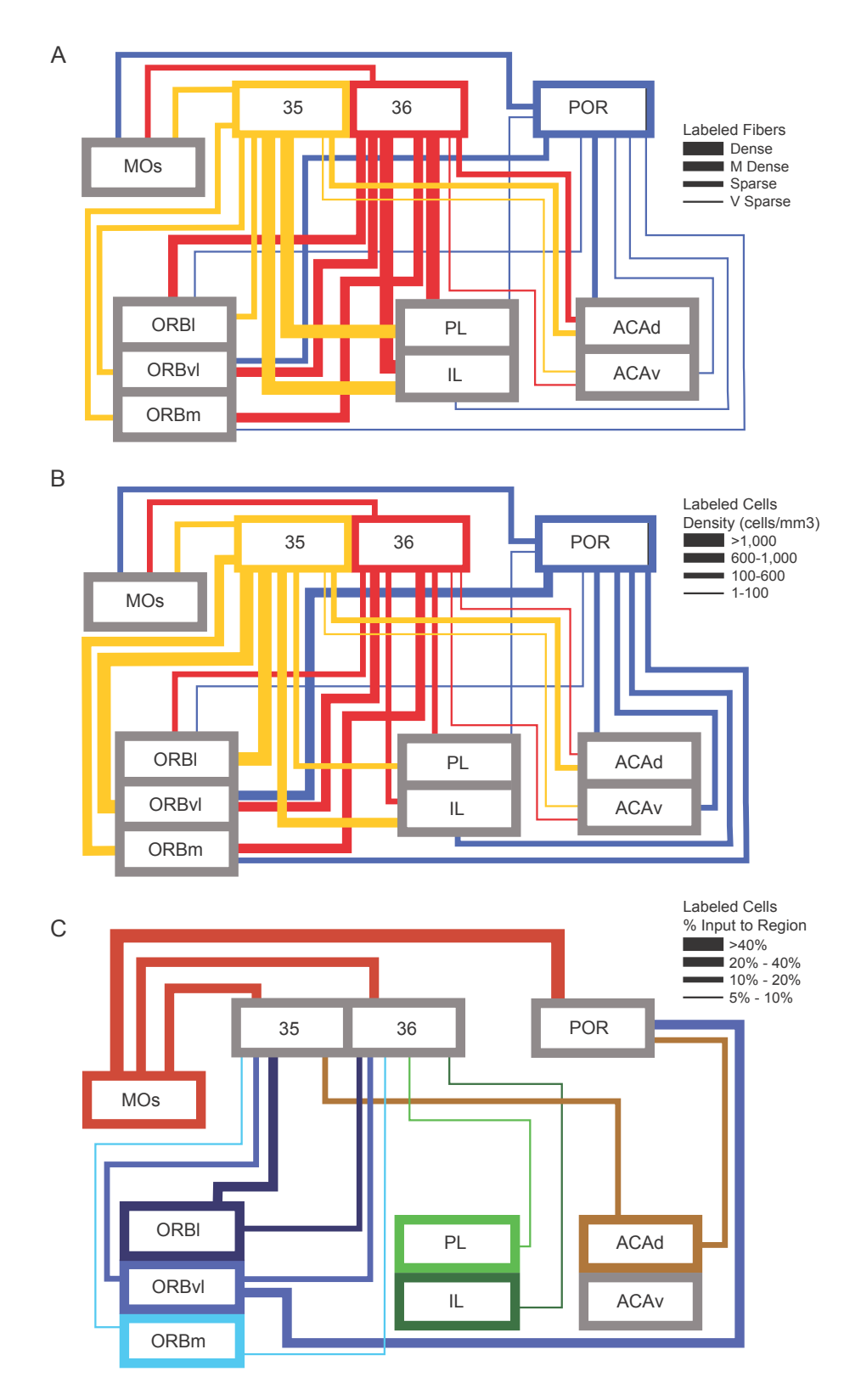


Figure 6. Summary of prefrontal efferents and afferents of PER areas 36 and 35 and the POR. A. Efferents based on density of anterograde fiber labeling. B. Afferents based on normalized densities of retrogradely labeled cells. C. Afferents based on percentage of total retrogradely labeled cells. For A and C, colors represent the origin of projections. For B, colors represent the termination of projections. Line thickness represents the strength of projections in densities and percentages.

Table 1. Anterograde Tracer Injection Sites

Location	Experiment	Layer	Size (µm)
Perirhinal Area 36			
Rostral area 36	54P	V-VI	400
Midrostrocaudal area 36	128B	II-VI	400
Caudal area 36	27P	II-VI	300
Ventral area 36	129B	II-V	300
Perirhinal Area 35			
Rostral area 35	24P	III-VI	300
Caudal area 35	16B	II-V	400
Postrhinal			
Rostral	39P	I-VI	400
Rostrodorsal	83B	IV-VI	500
Dorsal	134B	I-VI	500
Caudal	40P	III-VI	500

Anterograde injections sites are suffixed with a P or B for PHA-L and BDA, respectively.

Table 2. Retrograde Tracer Injection Sites

	Lavor	Siza (um)
Experiment	Layei	Size (µm)
440.55		400
–		400
120 FB	III-V	700
97 DY	III-V	500
98 DY	I-V	300
132 DY	V	200
94 FB	V	400
99 DY	11-111	300
100 DY	V	300
120 DY	V	300
102 DY	I-V	400
132 FB	I-VI	300
112 DY	V	400
108 FG	I-VI	300
97 FB	V	400
102 FB	V	200
98 FB	I-VI	600
100 FB	I-V	500
95 DY	III-VI	400
99 FB	I-V	500
	98 DY 132 DY 94 FB 99 DY 100 DY 120 DY 120 DY 132 FB 112 DY 108 FG 97 FB 102 FB 98 FB 100 FB 95 DY	119 FB I-V 120 FB III-V 97 DY III-V 98 DY I-V 132 DY V 94 FB V 99 DY II-III 100 DY V 120 DY V 102 DY I-V 132 FB I-VI 112 DY V 108 FG I-VI 97 FB V 98 FB I-VI 100 FB I-V 95 DY III-VI

Retrograde injection sites have the suffix DY, FB, or FG for Diamidino Yellow, Fast Blue and Fluoro-Gold.

Table 3. Density of Anterogradely Labeled Fibers

Efferent		Origin Regions		
Regions	Area 36	Area 35	POR	
ORBI	+++	++	+	
Layers I-III	++++	++	++	
Layer V	+++	++	+	
Layer VI	++	+	+	
ORBvI	+++	++	++	
Layers I-III	+++	++	++	
Layer V	+++		-	
Layer VI	++	++	-	
ORBm	+++	++	+	
Layers I-III	+++	++	+	
Layer V	+++	++	+	
Layer VI	+++	+	-	
IL	++++	++++	+	
Layers I-III	+++++	++++	+	
Layer V	++++	++++	-	
Layer VI	++	++	-	
PL	++++	++++	+	
Layers I-III	+++++	++++	+	
Layer V	++++	++++	+	
Layer VI	++	+	+	
ACAv	+	+	+	
Layers I-III	+	+	+	
Layer V	-	-	+	
Layer VI	-	-	+	
ACAd	++	++	++	
Layers I-III	++	++	+++	
Layer V	++	++	++	
Layer VI	-	-	+	
MOs	++	++	++	
Layers I-III	+++	+++	++	
Layer V	++	++	++	
Layer VI	+	+	+	

Data are average density of terminal fiber labeling across the efferent regions. See text for details of how fiber density was quantified. Legend: -, negligible; +, very sparse; ++, sparse; +++, moderately dense; ++++, dense; +++++, very dense.

Table 4. Density of Retrogradely Labeled Cells

Table 4. Delisity of Retrogradely Labeled Cells			
Afferent	Target Regions		
Regions	Area 36	Area 35	POR
ORBI	500	1699	32
Layers II-III	821	2514	41
Layer V	14	503	10
Layer VI	23	864	0
ORBvI	715	1315	767
Layers II-III	1329	1303	1095
Layer V	378	923	551
Layer VI	145	1545	157
ORBm	639	764	288
Layers II-III	1461	1584	385
Layer V	334	391	312
Layer VI	39	305	153
IL	374	718	126
Layers II-III	818	1671	130
Layer V	249	828	76
Layer VI	55	216	163
PL	126	262	44
Layers II-III	163	328	8
Layer V	166	328	48
Layer VI	32	142	71
ACAv	19	9	183
Layers II-III	4	17	31
Layer V	13	2	276
Layer VI	51	16	284
ACAd	99	108	423
Layers II-III	94	179	88
Layer V	138	83	684
Layer VI	45	76	333
MOs	148	259	175
Layers II-III	187	438	199
Layer V	163	182	414
Layer VI	40	121	74
Data are mean density of retrogradely-labeled cells			

Data are mean density of retrogradely-labeled cells per cubic millimeter for each structure. Note that densities are given in cells/mm³, and that smaller densities may represent such a small number of cells as to be considered negligible. Numbers in bold are the average densities for the entire region.

Table 5. Percentage of Retrogradely Labeled Cells

Afferent		Target Regions	
Regions	Area 36	Area 35	POR
ORBI	18	21	1
Layers II-III	90	85	79
Layer V	2	7	14
Layer VI	8	8	7
ORBvI	20	11	36
Layers II-III	66	43	53
Layer V	21	36	38
Layer VI	13	21	8
ORBm	9	5	2
Layers II-III	71	65	43
Layer V	26	30	45
Layer VI	3	5	12
IL	6	4	3
Layers II-III	48	64	27
Layer V	42	26	21
Layer VI	10	10	52
PL	9	4	0.1
Layers II-III	37	32	5
Layer V	56	53	54
Layer VI	7	15	41
ACAv	0.2	1	1
Layers II-III	25	43	11
Layer V	24	7	55
Layer VI	51	50	34
ACAd	4	13	10
Layers II-III	30	34	6
Layer V	56	46	74
Layer VI	15	20	20
MOs	34	40	47
Layers II-III	40	60	25
Layer V	54	32	63
Layer VI	6	8	12
Total Labeled Cells	5127±1450	8431±2878	5191±869

Data in bold print are mean percentage input to the target regions from the origins based on total normalized numbers of labeled cells arising from retrograde tracer injections. Data for layers are percentages of labeled cells for the particular region. Numbers of cells labeled in each region can be calculated from the estimated total number of labeled cells. Data are means±SEM.